Supplementary material for "Periodic migration in a physical model of cells on micropatterns"

Brian A. Camley, Yanxiang Zhao, Bo Li, Herbert Levine, and Wouter-Jan Rappel

1 Turning and bipedal motion

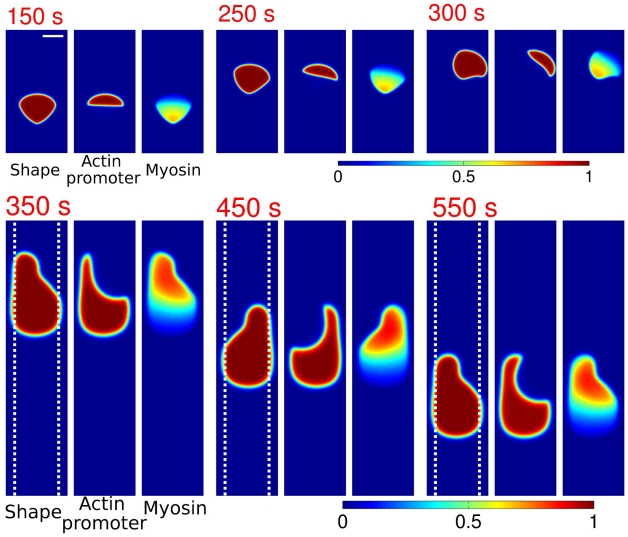

Figure S1: Many types of cell crawling appear, including bipedal motion and turning. Cell shape (phase field ϕ), actin promoter ($\rho_a\phi$), and myosin ($\rho_m\phi$) of cells at different times. Color plots are rescaled by 1, 1.4 μm^{-2}, and 0.8 μm^{-2}, respectively. TOP: Cell turning; total width of stripe is $w = 40$ μm (not in image; scale bar indicates 10 μm). BOTTOM: Bipedal motion. Total width of stripe is $w = 10$ μm (dashed lines).

2 Sharp interface derivation

We will derive the sharp interface results presented in the text. These are that the front and back interface velocities are given by $\pm\alpha\rho_a^{f,b} \mp \beta\rho_m^{f,b}$ with

$$\alpha = \frac{\eta_a^0}{4\nu_0}, \quad \beta = \frac{\eta_m^0 \ell_h}{2\nu_0}, \tag{S1}$$

where $\ell_h^2 = 2\nu_0/\xi$. In order to get these results, we will assume the sharp interface limit $\epsilon/\ell_h \ll 1$, and also that the cell's size L_{cell} is much larger than ℓ_h. We will also assume that the interface's curvature is not relevant.

Our Stokes equation for the cell's cytoskeletal velocity $\mathbf{u}$ is

$$\nabla \cdot \left[\nu(\phi)\left(\nabla\mathbf{u} + \nabla\mathbf{u}^T\right)\right] + \nabla\cdot\sigma_{\text{myo}} + \nabla\cdot\sigma_{\text{poly}} + \mathbf{F}_{\text{mem}} + \mathbf{F}_{\text{adh}} - \xi\mathbf{u} = 0 \tag{S2}$$

where $\nu(\phi) = \nu_0\phi(\mathbf{r})$ and the active stresses are given by

$$\sigma_{\text{myo}} = \eta_m^0\phi\rho_m\mathbf{I} \tag{S3}$$

$$\sigma_{\text{poly}} = -\eta_a^0\phi\rho_a\delta_\epsilon\hat{\mathbf{n}}\hat{\mathbf{n}} \tag{S4}$$

where $\mathbf{I}$ is the identity tensor, $\delta_\epsilon = \epsilon(\nabla\phi)^2$, and $\hat{\mathbf{n}}$ is the unit normal vector to the cell boundary. $\mathbf{F}_{\text{adh}}$ contains stochastic adhesion forces, which we ignore. We note that these adhesion forces may in some limits only renormalize ξ [1], so it may be appropriate to think of the

ξ as an effective value larger than that given in the simulation. The membrane forces are derived from a phase field approximation to the Helfrich energy and surface tension (see, e.g. [2, 3]), $\mathbf{F}_{\text{mem}} = \mathbf{F}_{\text{tension}} + \mathbf{F}_{\text{bend}}$ with

$$\mathbf{F}_{\text{tension}} = -\gamma \left(\epsilon \nabla^2 \phi - \frac{G'}{\epsilon} \right) \nabla \phi \tag{S5}$$

$$\mathbf{F}_{\text{bend}} = \kappa \epsilon \left(\nabla^2 - \frac{G''}{\epsilon^2} \right) \left(\nabla^2 \phi - \frac{G'}{\epsilon^2} \right) \nabla \phi \tag{S6}$$

where $G(\phi) = 18\phi^2(1-\phi)^2$ and G' and G'' denote derivatives of G with respect to ϕ.

We are interested in creating an effectively one-dimensional model. We approximate our cell's complex shape by an effectively one-dimensional front that minimizes the tension and bending energies (i.e. $\mathbf{F}_{\text{tension}} = \mathbf{F}_{\text{bend}} = 0$). This will be true if $\epsilon \nabla^2 \phi = \frac{G'}{\epsilon}$, or (for a front in the y direction)

$$\phi_I(y) = \frac{1}{2}\left(1 + \tanh(3y/\epsilon)\right) \tag{S7}$$

Under this assumption, the Stokes equation becomes

$$\tilde{\nu} \partial_y \left[\phi_I(y) \partial_y u \right] + F_{\text{myo}}\left[\phi_I\right] + F_{\text{poly}}\left[\phi_I\right] - \xi u = 0 \tag{S8}$$

where $\tilde{\nu} = 2\nu_0$, $F_{\text{poly}} \equiv \partial_y \sigma_{\text{poly}}$ and $F_{\text{myo}} \equiv \partial_y \sigma_{\text{myo}}$ We will look at the two force terms separately, since this equation is linear and we can superimpose the two resulting velocity fields. We will also assume that the densities ρ_a and ρ_m do not vary quickly at the front, so that $F_{\text{poly}} \approx -\eta_a^0 \rho_a \partial_y(\phi_I \delta_\epsilon)$ and $F_{\text{myo}} \approx \eta_m^0 \rho_m \partial_y \phi_I$. We illustrate the resulting field ϕ_I and the forces in Fig. S2 below.

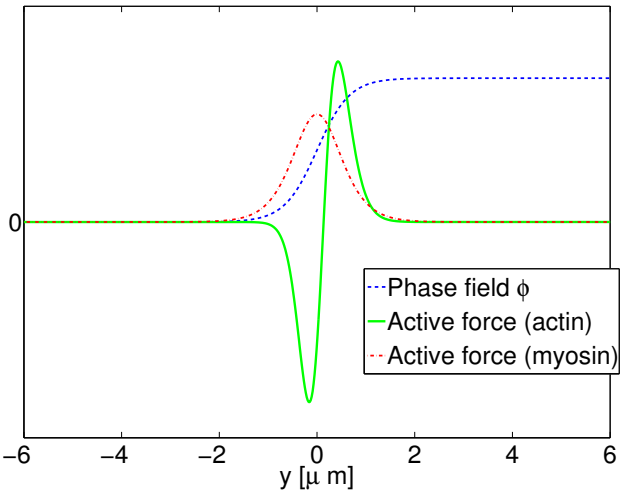

Figure S2: We show the phase field and active forces at the interface at $y = 0$. Here the phase field $\phi_I = \frac{1}{2}\left(1 + \tanh(3y/\epsilon)\right)$. The active force due to actin polymerization is $F_{\text{poly}} \approx -\eta_a^0 \rho_a \partial_y(\phi_I \delta_\epsilon)$ and the active force due to myosin contractility is $F_{\text{myo}} \approx \eta_m^0 \rho_m \partial_y \phi_I$. $\epsilon = 2\mu$m in this figure.

2.1 Active force due to actin polymerization

We start by rewriting Eq. S8 with $F_{\text{poly}} = -\eta_a^0 \rho_a \partial_y(\phi_I \delta_\epsilon)$ and $F_{\text{myo}} = 0$. (We will use linearity to rescue the complete result later.) Rescaling our lengths to $r = y/(\ell_h)$ where $\ell_h^2 = \tilde{\nu}/\xi$ and defining $\delta = \epsilon/3\ell_h$, we find

$$\partial_r \left[\{1 + \tanh(r/\delta)\} \partial_r u \right] - \frac{\chi}{\delta} \partial_r \left[\{1 + \tanh(r/\delta)\} \operatorname{sech}^4(r/\delta) \right] - 2u = 0 \tag{S9}$$

where $\chi = \frac{3}{4}\eta_a^0 \rho_a / \tilde{\nu}$. We can't solve this equation exactly, but can develop an asymptotic approximation in the sharp interface limit of $\epsilon \ll \ell_h$ ($\delta \ll 1$). In particular, we can see that in the sharp interface limit, the term $\operatorname{sech}^4 r/\delta$ can be neglected everywhere but near the front position, $r = O(\delta)$. Moving to the stretched variable $z = r/\delta$, and defining $U(z) = u(r)$ for convenience,

$$\partial_z \left[(1 + \tanh z) \partial_z U \right] - \chi \partial_z \left[(1 + \tanh z) \operatorname{sech}^4 z \right] - 2\delta^2 U = 0 \tag{S10}$$

To $O(\delta^0)$, we can neglect the last term on the right. The remaining ODE can be directly integrated:

$$U(z) = A\left(z - \frac{1}{2} e^{-2z} \right) + B + \chi \left\{ \frac{4}{(1+e^{-2z})^2} - \frac{8}{3(1+e^{-2z})^3} \right\} \tag{S11}$$

We cannot consistently apply the boundary conditions $u(r \to \pm\infty) = 0$ to this solution; we need to match it to the solution in the outer region. However, the outer regions to the right and left of the front have two distinctly different characters. For $r \gg \delta$, $1+\tanh(r/\delta) \approx 2$, and the outer expansion is

$$\partial_r^2 u_R - u_R = 0 \tag{S12}$$

and we can immediately determine $u_R = Ce^{-r}$, neglecting the solution that diverges as $r \to \infty$. Matching to the interior solution yields the requirement $C = B + \frac{4}{3}\chi$ and $A = -\delta C$. However, for $r \ll -\delta$, $1 + \tanh(r/\delta)$ approaches zero; δ is a singular perturbation to the outer equation in the left region. For $r \ll -\delta$, $1 + \tanh(r/\delta) \approx 2e^{2r/\delta}$, and so

$$\partial_r(e^{2r/\delta}\partial_r u_L) - u_L = 0 \tag{S13}$$

which can be solved to find

$$u_L = De^{-r/\delta}K_1(\delta e^{-r/\delta}) \tag{S14}$$

where K_1 is the modified Bessel function of order 1, and we have dropped the solution that diverges as $r \to -\infty$. To match this to the interior solution, we choose $r = \delta z_c$ with z_c fixed but large (and negative), and look at the behavior as $\delta \to 0$:

$$u_L \sim D\left[\frac{1}{\delta} + \frac{e^{-2z_c}}{2}\delta\left\{\ln\delta - z_c - \ln 2 + \gamma_E - 1/2\right\}\right] \tag{S15}$$

$$\sim D\left[\frac{1}{\delta} + \frac{e^{-2z_c}}{2}\delta\ln\delta\right] \tag{S16}$$

where γ_E is the Euler gamma, $\gamma_E = 0.5772\ldots$. We match to the interior solution at $z = z_c$ with $z_c \ll -1$,

$$U \sim -\frac{1}{2}Ae^{-2z_c} + B \tag{S17}$$

Matching then requires that $-A = D\delta\ln\delta$ and $B = D/\delta$. Combining this with our earlier matching requirements, $C = B + \frac{4}{3}\chi$ and $A = -\delta C$, we find:

$$A/\chi = \frac{4}{3}\frac{\delta^2\ln\delta}{1-\delta\ln\delta} \tag{S18}$$

$$B/\chi = -\frac{4}{3}\frac{1}{1-\delta\ln\delta} \tag{S19}$$

$$C/\chi = -\frac{4}{3}\frac{\delta\ln\delta}{1-\delta\ln\delta} \tag{S20}$$

$$D/\chi = -\frac{4}{3}\frac{\delta}{1-\delta\ln\delta} \tag{S21}$$

Importantly, because $C \to 0$ as $\delta \to 0$, in the sharp interface limit, there is no long-range velocity induced by the actin promoter at the interface.

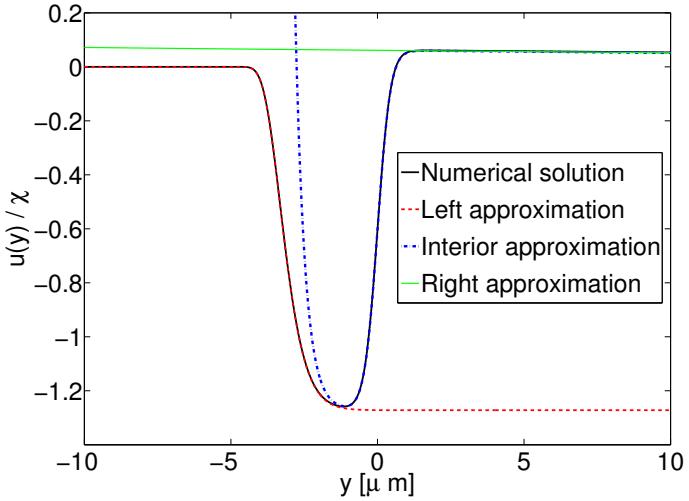

Figure S3: Velocity of fluid due to the presence of actin promoter at the cell boundary. Interface is at $y = 0$ as above, i.e. $\phi = \frac{1}{2}\left[1 + \tanh(3y/\epsilon)\right]$. Here $\epsilon = 2$ μm, $\ell_h = 63$ μm, i.e. $\delta \approx 0.01$.

Our asymptotics provide an excellent approximation to the full numerical solution (Fig. S3). It also allows us to determine the interface velocity, $u(0)$ (using the interior solution). We find in the sharp interface limit that

$$u_{\text{interface}} = -\frac{2}{3}\chi \equiv -\alpha\rho_a \tag{S22}$$

where

$$\alpha = \frac{\eta_a^0}{2\tilde{\nu}} = \frac{\eta_a^0}{4\nu_0}. \tag{S23}$$

This is the result given in the main paper. It is only the leading order term; higher-order terms that depend on δ can also be obtained from the solution above. The process for myosin is very similar, but we will find that a long-range (on the order of ℓ_h) velocity will be induced, unlike the actin promoter case.

2.2 Myosin force

We start by rewriting Eq. S8 with $F_{\text{myo}} = \eta_m^0\rho_m\partial_y\phi$ and $F_{\text{poly}} = 0$. Rescaling our lengths to $r = y/(\ell_h)$ where $\ell_h^2 = \tilde{\nu}/\xi$ and defining $\delta = \epsilon/3\ell_h$, we find

$$\partial_r\left[\{1+\tanh(r/\delta)\}\,\partial_r u\right] + \mu\partial_r\left[1+\tanh(r/\delta)\right] - 2u = 0 \tag{S24}$$

where $\mu = \eta_m^0\rho_m\ell_h/\tilde{\nu}$. Note that unlike χ in the actin promoter case, μ does have an explicit dependence on the hydrodynamic length scale ℓ_h.

We develop an asymptotic approximation in the sharp interface limit of $\epsilon \ll \ell_h$ ($\delta \ll 1$). Moving to the stretched variable $z = r/\delta$, and defining $U(z) = u(r)$,

$$\partial_z\left[(1+\tanh z)\partial_z U\right] + \mu\delta\partial_z\left[1+\tanh z\right] - 2\delta^2 U = 0 \tag{S25}$$

To linear order in δ, the last term can be dropped, and the remaining equation can be easily integrated to find

$$U(z) = A\left(z - \frac{1}{2}e^{-2z}\right) + B - \frac{\mu\delta}{2}e^{-2z} \tag{S26}$$

The outer limits are the same as in the actin promoter case. We then get the matching conditions $D/\delta = B$, $A+\mu\delta = -D\delta\ln\delta$, $B = C$, and $A = -\delta C$. These can be solved to find

$$A/\mu = -\frac{\delta}{1-\delta\ln\delta} \tag{S27}$$

$$B/\mu = \frac{1}{1-\delta\ln\delta} \tag{S28}$$

$$C/\mu = \frac{1}{1-\delta\ln\delta} \tag{S29}$$

$$D/\mu = \frac{\delta}{1-\delta\ln\delta} \tag{S30}$$

Note that C does not vanish in the sharp interface limit: the presence of myosin at the interface leads to a velocity far away from the interface, $u(r) \approx \mu e^{-r}$. Our asymptotic approximations are again an excellent approximation to the full numerical solution (Fig. S4).

In the sharp interface limit, $u(0)$ becomes

$$u_{\text{interface}} = \mu \equiv \beta\rho_m \tag{S31}$$

where

$$\beta = \frac{\eta_m^0\ell_h}{\tilde{\nu}} = \frac{\eta_m^0\ell_h}{2\nu_0} \tag{S32}$$

2.3 When can we apply the sharp interface result?

We argue that in the limit $L_{\text{cell}} \gg \ell_h$, we can neglect correlations between the cell edges. We have been attempting to determine the velocity of the cell interface using only the actin promoter and myosin densities at the interface, but no information about the actin promoter and myosin throughout the cell, or the other interface of the cell. When is this appropriate? We have seen above that myosin at the cell interface induces a velocity in the cell body with a dependence of position of e^{-y/ℓ_h}; if $L_{\text{cell}} \gg \ell_h$, one interface will not affect the other. We have also neglected forces coming from *internal* gradients of the myosin-induced stress; once again, the characteristic length scale for these forces is ℓ_h, and so they should not affect the velocity of the interfaces if $L_{\text{cell}} \gg \ell_h$. The sharp interface results could be generalized to include all of these effects, but they produce additional complications, such as the need to track the details of myosin within the cell.

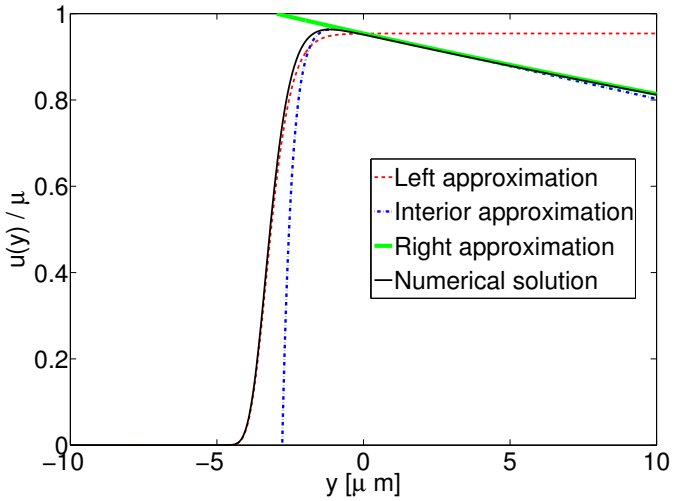

Figure S4: Velocity of fluid due to the presence of myosin at the cell boundary. Interface is at $y = 0$ as above, i.e. $\phi = \frac{1}{2}[1 + \tanh(3y/\epsilon)]$. Here $\epsilon = 2$ μm, $\ell_h = 63$ μm, i.e. $\delta \approx 0.01$. Note that even though δ is small, the velocity to the right of the interface is not small since C is $O(\delta^0)$.

3 Tables of parameters used

3.1 Parameters used for all two-dimensional phase field simulations

We mark with an asterisk the parameters that have been changed from the simulations presented in Ref. [3]. Parameters were originally chosen in [3] to ensure that the cell velocity, actin flow velocity, and midline stress were close to experimentally reported values for keratocytes; in general, we have attempted not to change these values. Where possible, we have given literature justification for these parameters.

3.1.1 Phase field and cell boundary properties

Parameter	Description	Value	Justification
γ	Cell tension coefficient	20 pN	Order-of-magnitude set in [4]
κ	Cell bending coefficient	20 pN μm^2	Order-of-magnitude set in [4]
ϵ	Phase field width	2 μm	Chosen to ensure smooth variation in ϕ
Γ	Phase field relaxation parameter	0.4 μm/s	Set in [3]

3.1.2 Cytoskeletal flow parameters

Parameter	Description	Value	Justification
ν_0	Viscosity of cytoskeletal flow	10^3 pN s / μm	Set roughly by [5]; see also [6]
η_a^0	Protrusion coefficient	560 pN μm ^{2}	Chosen to reproduce shapes and other features in [3]
η_m^0	Myosin contractility coefficient	60-61 pN μm *	Similar to that of [6]; tuned to increase periodic migration amplitude
ξ	Substrate friction coefficient	0.5 Pa s / μm	Value arising from cell sitting on layer of water with height 2 nm [7]

3.1.3 Reaction-diffusion parameters

In the same wave-pinning kinetics as [3] for the reaction term in the actin promoter equation,

$$f(\rho_a, \rho_a^{\text{cyt}}) = k_b \left(\frac{\rho_a^2}{K_a^2 + \rho_a^2} + k_a \right) \rho_a^{\text{cyt}} - k_c \rho_a \tag{S33}$$

where, by the conservation of total actin promoter, $\int d^2r \left(\rho_a(\mathbf{r}) + \rho_a^{\text{cyt}}\right)\phi(\mathbf{r}) = N_a^{\text{tot}}$, or, assuming the cytosolic actin promoter is well-mixed (uniform),

$$\rho_a^{\text{cyt}} = \frac{N_a^{\text{tot}} - \int d^2r \rho_a(\mathbf{r})\phi(\mathbf{r})}{\int d^2r \phi(\mathbf{r})}. \tag{S34}$$

We note that this formula was written incorrectly in the Supplementary Material of Ref. [3].

Parameter	Description	Value	Justification
k_a	Unitless base activation rate	0.01 [a]	Order-of-magnitude from [8]
k_b	Overall activation rate	10 s^{-1}	Order-of-magnitude from [8]
k_c	Deactivation rate	10 s^{-1}	Order-of-magnitude from [8]
K_a	Positive feedback threshold for actin promoter concentration	1 μm^{-2}	Order-of-magnitude from [8]
D_a	Actin promoter diffusion coefficient	0.8 $\mu\text{m}^2/\text{s}$	Typical membrane-bound protein diffusion coefficient [9]
D_m^0	Myosin diffusion coefficient at zero actin concentration	2 $\mu\text{m}^2/\text{s}$	Chosen in [3]
K_D	Myosin diffusion threshold, $D_m = D_m^0/(1+\rho_a/K_D)$	0.5 μm^{-2} [b]	Chosen in [3]
N_a^{tot}	Total amount of actin promoter	485* [c]	Roughly rescaled by cell size from value chosen in [3] proportional to cell area
ρ_m^0	Initial density of myosin	0.3 μm^{-2}	Chosen such that myosin stress corresponds to that estimated in [6]

3.1.4 Adhesion parameters

Parameter	Description	Value	Justification
N_{adh}	Number of adhesions	1000* [d]	Roughly rescaled from value chosen in [3] proportional to cell area
F_{grip}^0	Characteristic gripping stress for gripping-slipping rupture	5 Pa	Chosen in [3] to reproduce traction forces and shape of keratocytes
k_{grip}^0	Gripping coefficient	2.5 Pa / (s μm)	Chosen in [3] to reproduce traction forces and shape of keratocytes
k_{slip}^0	Slipping coefficient	0.25 Pa / μm	Chosen in [3] to reproduce traction forces and shape of keratocytes
r_{on}	Rate of transition from slipping to gripping state	0.005 s^{-1}	Chosen in [3] to reproduce traction forces and shape of keratocytes
r_{off}^0	Rate of transition from gripping to slipping state (at zero force)	0.002 s^{-1}	Chosen in [3] to reproduce traction forces and shape of keratocytes
r_{die}	Rate of slipping site death	0.2 s^{-1}	Chosen in [3] to reproduce traction forces and shape of keratocytes

3.1.5 Numerical evaluation parameters

Parameter	Description	Value
$n \times m$	Number of (horizontal, vertical) grid points	256×256
$L_x \times L_y$	Box size	$50\mu\text{m} \times 50\mu\text{m}$
Δt	Time step	2×10^{-3} s*
λ	Cutoff for evaluating phase field equations	10^{-4}

3.2 Parameters used for each figure

3.2.1 Figure 1

For the oscillation in Fig. 1, we start with an initial state of a circular cell with radius 6 μm. We choose $\eta_m^0 = 61$ pN μm, and have an adhesive stripe of total width $w = 6\mu\text{m}$, i.e. $\chi(\mathbf{r}) = \frac{1}{2}\left[1 + \tanh(3\{\frac{w}{2} - |x|\}/\epsilon)\right]$. All other parameters are as written in the tables above.

[a] The units for this parameter were listed incorrectly in the Supplemental Material of Ref. [3].

[b] This is the value used in Ref. [3], though it was listed incorrectly in the Supplemental Material of that work.

[c] This parameter is denoted by ρ_a^{tot} in Ref. [3].

[d] This describes the total number of adhesions over the entire cell. The value of N_{adh} in Ref. [3] is listed incorrectly, and should be $N_{\text{adh}} = 4000$ over the whole cell. The change in adhesion number in this paper roughly corresponds to the change in cell area.

3.2.2 Figure 2

We think of our one-dimensional model as describing a slice down the center of a two-dimensional cell with width w, but with ρ_a uniform across the x direction. Parameters for the actin promoter reaction-diffusion part of the one-dimensional model are exactly the same as for the two-dimensional model of Fig. 1; however, the conservation law follows a slightly different form:

$$\int_{-w/2}^{w/2} dx \int_{-L_y/2}^{L_y/2} \left[\rho_a(y) + \rho_a^{\text{cyt}}\right] \phi(y) = N_a^{\text{tot}} \tag{S35}$$

or, equivalently,

$$\rho_a^{\text{cyt}} = \frac{N_a^{\text{tot}}/w - \int dy \rho_a(y)\phi(y)}{\int dy \phi(y)}. \tag{S36}$$

The parameters unique to the one-dimensional model are $\alpha = 0.14\mu\text{m}^3/\text{s}$ and $\beta = 0.068\mu\text{m}^3/\text{s}$, $m_0 = 2.43\mu\text{m}^{-2}$ and $\tau = 30$ s. The value for α is determined by the sharp interface result, $\alpha = \eta_a^0/4\nu_0$, using the two-dimensional simulation parameters. We have set β, m_0, and τ so that the cell oscillates similarly to the two-dimensional simulation. The one-dimensional model is evaluated on a grid of 512 points with $L_y = 100$ μm, with $\Delta t = 0.01$ s.

3.2.3 Figure S1

For the turning motion (Fig. S1 top), we start with an initial state of a circular cell with radius 8 μm. We choose $\eta_m^0 = 60$ pN μm, and have an adhesive stripe of total width $w = 40$ μm, i.e. $\chi(\mathbf{r}) = \frac{1}{2}\left[1 + \tanh(3\{\frac{w}{2} - |x|\}/\epsilon)\right]$. For the bipedal motion (Fig. S1 bottom), we choose exactly the same parameters, except that we take $w = 10$ μm. All other parameters are as written in the tables above.

3.3 Robustness of periodic migration to variation in parameters

The bulk of our parameters have been set by comparison with experiments on keratocytes, and are identical to those used in [3]; they were not selected to observe periodic migration. However, some parameters have been changed in order to ensure that the cells polarize and migrate on stripes. In particular, we changed N_a^{tot} and N_{adh} because the cells we study are significantly smaller in area than those in [3]. We also changed η_m^0 to change the contraction speed and vary the amplitude of periodic migration. Initial simulations have shown that periodic migration can be observed over wider ranges of parameters as well; varying one parameter at a time, we see periodic migration at $N_{\text{adh}} = 700$, or $\eta_m^0 = 80$ pN μm, or $N_a^{\text{tot}} = 400$. These parameters can be changed more if we change multiple parameters at once. Our experience with altering the model suggests that periodic migration can be re-created as long as the central polarization mechanism is in place, the contraction and protrusion are closely balanced, and the myosin effectively keeps the memory.

4 Details of numerical algorithm

4.1 Time-stepping and discretization

Our goal is to numerically solve the system of equations

$$\partial_t \phi + \mathbf{u}\cdot\nabla\phi = \Gamma(\epsilon\nabla^2\phi - G'(\phi)/\epsilon + \epsilon c|\nabla\phi|) \tag{S37}$$

$$\partial_t(\phi\rho_a) + \nabla\cdot(\phi\rho_a\mathbf{u}) = \nabla\cdot(\phi D_a\nabla\rho_a) + \phi f(\rho_a, \rho_a^{\text{cyt}}) \tag{S38}$$

$$\partial_t(\phi\rho_m) + \nabla\cdot(\phi\rho_m\mathbf{u}) = \nabla\cdot(\phi D_m(\rho_a)\nabla\rho_a) \tag{S39}$$

$$\nabla\cdot\left[\nu_0\phi(\nabla\mathbf{u} + \nabla\mathbf{u}^T)\right] + \nabla\cdot(\sigma_{\text{poly}} + \sigma_{\text{myo}}) + \mathbf{F}_{\text{mem}} + \mathbf{F}_{\text{adh}} - \xi\mathbf{u} = 0 \tag{S40}$$

We fix a uniform spatial grid with grid sizes Δx, Δy. We also use a fixed time step Δt to march these equations forward from initial conditions $\phi^{(0)}, \mathbf{u}^{(0)}, \rho_a^{(0)}, \rho_m^{(0)}$. We denote the state of the system at time $t = n\Delta t$ by $\phi^{(n)}, \mathbf{u}^{(n)}, \rho_a^{(n)}, \rho_m^{(n)}$. Suppose we have obtained all these quantities at the time $n\Delta t$. We then solve all the equations (S37)–(S39) to obtain these quantities at the time $(n+1)\Delta t$.

We first obtain $\phi^{(n+1)}$ from the ϕ-equation (S37) with the forward Euler scheme:

$$\phi^{(n+1)} = \phi^{(n)} - \Delta t\,\mathbf{u}^{(n)}\cdot\nabla\phi^{(n)} + \Delta t\,\Gamma\left[\epsilon\nabla^2\phi^{(n)} - G'(\phi^{(n)})/\epsilon + \epsilon c^{(n)}|\nabla\phi^{(n)}|\right].$$

On the right-hand side of this equation, $\nabla\phi^{(n)}$ is calculated with a central difference scheme, $\nabla^2\phi^{(n)}$ is calculated by five-point finite difference scheme, and the curvature term $c^{(n)}$ is calculated by

$$c^{(n)} = \nabla\cdot\frac{\nabla\phi^{(n)}}{|\nabla\phi^{(n)}|}$$

when $|\nabla\phi^{(n)}| > 0.01$, and set to be zero otherwise.

We next solve Eq. (S38) and Eq. (S39) to obtain $\rho_a^{(n+1)}$ and $\rho_m^{(n+1)}$, respectively. We apply the forward Euler scheme to the reaction-diffusion-advection equation (S38):

$$\phi^{(n)}\frac{\rho_a^{(n+1)}-\rho_a^{(n)}}{\Delta t}+\frac{\phi^{(n+1)}-\phi^{(n)}}{\Delta t}\rho_a^{(n)}=-\nabla\cdot(\phi^{(n)}\rho_a^{(n)}\mathbf{u}^{(n)})+\nabla\cdot(\phi^{(n)}D_a\nabla\rho_a^{(n)})+\phi^{(n)}f^{(n)}$$

Equivalently,

$$\rho_a^{(n+1)}=\frac{(2\phi^{(n)}-\phi^{(n+1)})}{\phi^{(n)}}\rho_a^{(n)}-\Delta t\frac{\nabla\cdot(\phi^{(n)}\rho_a^{(n)}\mathbf{u}^{(n)})}{\phi^{(n)}}+\Delta t\frac{\nabla\cdot(\phi^{(n)}D_a\nabla\rho_a^{(n)})}{\phi^{(n)}}+\Delta t f^{(n)} \tag{S41}$$

We only divide by $\phi^{(n)}$ in the region where $\phi^{(n)}\geq\lambda$, where $\lambda=10^{-4}$. Outside of this region, we keep $\rho_a^{(n+1)}=\rho_a^{(n)}$. More specifically, we have use the following discretization:

$$\begin{aligned}
\left[\nabla\cdot(\phi^{(n)}\rho_a^{(n)}\mathbf{u}^{(n)})\right]_{ij} &= \left[\phi^{(n)}_{i+1/2,j}\rho^{(n)}_{a,i+1/2,j}u^{(n)}_{i+1/2,j}-\phi^{(n)}_{i-1/2,j}\rho^{(n)}_{a,i-1/2,j}u^{(n)}_{i-1/2,j}\right]\Big/\Delta x\\
&\quad+\left[\phi^{(n)}_{i,j+1/2}\rho^{(n)}_{a,i,j+1/2}v^{(n)}_{i,j+1/2}-\phi^{(n)}_{i,j-1/2}+\rho^{(n)}_{a,i,j-1/2}v^{(n)}_{i,j-1/2}\right]\Big/\Delta y\\
\left[\nabla\cdot(\phi^{(n)}D_a\nabla\rho_a^{(n)})\right]_{ij} &= D_a\left[\phi^{(n)}_{i+1/2,j}\frac{\rho^{(n)}_{a,i+1,j}-\rho^{(n)}_{a,ij}}{\Delta x}-\phi^{(n)}_{i-1/2,j}\frac{\rho^{(n)}_{a,ij}-\rho^{(n)}_{a,i-1,j}}{\Delta x}\right]\Big/\Delta x\\
&\quad+D_a\left[\phi^{(n)}_{i,j+1/2}\frac{\rho^{(n)}_{a,i,j+1}-\rho^{(n)}_{a,ij}}{\Delta y}-\phi^{(n)}_{i,j-1/2}\frac{\rho^{(n)}_{a,ij}-\rho^{(n)}_{a,i,j-1}}{\Delta y}\right]\Big/\Delta y
\end{aligned}$$

where $\mathbf{u}_{ij}^{(n)}=\left(u_{ij}^{(n)},v_{ij}^{(n)}\right)$. We apply the analogous forward Euler scheme to the ρ_m-equation (S39). Since the diffusion coefficient $D_m=D_m(\rho_a)$ depends on ρ_a, we discretize the diffusion term at a grid point labeled by (i,j) as follows

$$\begin{aligned}
&\left[\nabla\cdot(\phi^{(n)}D_m^{(n)}\nabla\rho_a^{(n)})\right]_{ij}\\
&=\left[\frac{\phi^{(n)}_{ij}D^{(n)}_{m,ij}+\phi^{(n)}_{i+1,j}D^{(n)}_{m,i+1,j}}{2}\cdot\frac{\rho^{(n)}_{a,i+1,j}-\rho^{(n)}_{a,ij}}{\Delta x}-\frac{\phi^{(n)}_{ij}D^{(n)}_{m,ij}+\phi^{(n)}_{i-1,j}D^{(n)}_{m,i-1,j}}{2}\cdot\frac{\rho^{(n)}_{a,ij}-\rho^{(n)}_{a,i-1,j}}{\Delta x}\right]\Big/\Delta x\\
&+\left[\frac{\phi^{(n)}_{ij}D^{(n)}_{m,ij}+\phi^{(n)}_{i,j+1}D^{(n)}_{m,i,j+1}}{2}\cdot\frac{\rho^{(n)}_{a,i,j+1}-\rho^{(n)}_{a,ij}}{\Delta y}-\frac{\phi^{(n)}_{ij}D^{(n)}_{m,ij}+\phi^{(n)}_{i,j-1}D^{(n)}_{m,i,j-1}}{2}\cdot\frac{\rho^{(n)}_{a,ij}-\rho^{(n)}_{a,i,j-1}}{\Delta y}\right]\Big/\Delta y
\end{aligned}$$

where $D^{(n)}_{m,ij}=D_m(\rho^{(n)}_{a,ij})$. To keep ρ_m conserved and reduce its drift, we rescale ρ_m at each time step so that the total integral of ρ_m is kept a constant. We note that we have corrected the position of the non-constant diffusion coefficient in the ρ_m equation in [3].

Finally, we solve the Stokes equation (S40) with a semi-implicit Fourier spectral scheme to obtain $\mathbf{u}^{(n+1)}$. To do so, we first subtract the term $\nu_0\tilde{\phi}\nabla^2\mathbf{u}$ from both sides of the Stokes equation (S40) with $\tilde{\phi}$ a constant (e.g., $\tilde{\phi}=2$) to yield

$$\xi\mathbf{u}-\nu_0\tilde{\phi}\nabla^2\mathbf{u}=\nabla\cdot\left[\nu_0(\phi-\tilde{\phi})\nabla\mathbf{u}+\nu_0\phi\nabla\mathbf{u}^T)\right]+\nabla\cdot(\sigma_{\text{poly}}+\sigma_{\text{myo}})+\mathbf{F}_{\text{mem}}+\mathbf{F}_{\text{adh}}\equiv\text{RHS}(\mathbf{u},\phi,\rho_a,\rho_m)$$

To obtain $\mathbf{u}^{(n+1)}$, we set $\mathbf{u}_0^{(n+1)}=\mathbf{u}^{(n)}$ and solve the following equation iteratively using the spectral Fourier method:

$$\xi\mathbf{u}_{k+1}^{(n+1)}-\nu_0\tilde{\phi}\nabla^2\mathbf{u}_{k+1}^{(n+1)}=\text{RHS}(\mathbf{u}_k^{(n+1)},\phi^{(n+1)},\rho_a^{(n+1)},\rho_m^{(n+1)})\qquad k=0,1,\ldots,m$$

and set $\mathbf{u}^{(n+1)}=\mathbf{u}_m^{(n+1)}$. The calculations of $\nabla\cdot(\sigma_{\text{poly}}+\sigma_{\text{myo}})$, $\mathbf{F}_{\text{mem}}$ and $\mathbf{F}_{\text{adh}}$ are performed as in [3]. The number of steps m in this iteration is set to be $m=10$ or set by

$$\max|\mathbf{u}_m^{(n+1)}-\mathbf{u}_{m-1}^{(n+1)}|<0.01\ \max|\mathbf{u}_m^{(n+1)}|.$$

Shifting of the simulation box when the cell approaches the box edges is performed as in [3, 4].

4.2 Adhesion dynamics and calculation of adhesion force

The adhesion dynamics are precisely as given in [3], except that adhesions do not form off of the adhesive stripe, and are destroyed if they leave the stripe. For completeness, we summarize these dynamics here.

Adhesions between the cell and substrate are tracked individually; there are a fixed number N_{adh} of adhesions, and if one is destroyed, another one is created. The probability of adhesion formation is proportional to ρ_a and to ϕ, resulting in nascent adhesions being more likely to form at the front of the cell. We compute the initial adhesion location by a rejection method: we propose an adhesion location

$\mathbf{r}_0$ distributed uniformly in the region $|x| \leq \frac{w}{2}$, where w is the total width of the adhesive stripe, and accept that adhesion location with probability $p = \rho_a(\mathbf{r}_0)\phi/\max(\rho_a)$. Adhesions are destroyed if they leave the stripe (i.e. have $|x| > \frac{w}{2}$) or if $\phi < 1/2$ at the adhesion location.

Adhesions are advected by the cytoskeletal flow, $\mathbf{u}$; in practice, we choose the adhesion velocity to be the velocity $\mathbf{u}$ at the nearest grid point to the adhesion location.

Adhesions have two modes: "slipping" and "gripping." Adhesions are formed in gripping mode. When an adhesion is formed or transitions into gripping mode, its initial position $\mathbf{r}_0$ is noted. The gripping adhesion acts as a spring stretched from its initial location (where the adhesion attaches to the substrate) to its current location. It thus exerts a force on the cell of

$$\mathbf{F}_{\text{grip}} = -k_{\text{grip}}(\mathbf{r} - \mathbf{r}_0) \tag{S42}$$

By contrast, a slipping adhesion exerts a force

$$\mathbf{F}_{\text{slip}} = -k_{\text{slip}}\mathbf{u}(\mathbf{r}) \tag{S43}$$

where $\mathbf{r}$ is the adhesion position. We assume that the adhesions mature over time: $k_{\text{grip}} = k^0_{\text{grip}} t_{\text{adh}}$ and $k_{\text{slip}} = k^0_{\text{slip}} t_{\text{adh}}$ where t_{adh} is the age of the adhesion site. Adhesions may transition between slipping and gripping, and slipping adhesions may disappear. Gripping adhesions rupture and become slipping adhesions with a force-dependent rate $r_{\text{off}} = r^0_{\text{off}} \exp(|\mathbf{F}_{\text{grip}}|/F_0)$, with F_0 the gripping strength scale. Slipping adhesions may return to gripping mode with a rate r_{on}, and disappear with a rate r_{die}. To calculate the force density $\mathbf{F}_{\text{adh}}$ that enters into the Stokes equation, forces on adhesions are distributed to the nearest grid point; we therefore list the appropriate units in terms of forces per unit area. (We note that [3] incorrectly describes the force as being spread over the closest four grid points.)

References

[1] Sam Walcott and Sean X. Sun. A mechanical model of actin stress fiber formation and substrate elasticity sensing in adherent cells. *Proceedings of the National Academy of Sciences*, 107(17):7757, 2010.

[2] Qiang Du, Chun Liu, Rolf Ryham, and Xiaoqiang Wang. Energetic variational approaches in modeling vesicle and fluid interactions. *Physica D: Nonlinear Phenomena*, 238(9):923–930, 2009.

[3] Danying Shao, Herbert Levine, and Wouter-Jan Rappel. Coupling actin flow, adhesion, and morphology in a computational cell motility model. *Proceedings of the National Academy of Sciences*, 109(18):6851, 2012.

[4] Danying Shao, Wouter-Jan Rappel, and Herbert Levine. Computational model for cell morphodynamics. *Physical Review Letters*, 105(10):108104, 2010.

[5] Andreas R Bausch, Florian Ziemann, Alexei A Boulbitch, Ken Jacobson, and Erich Sackmann. Local measurements of viscoelastic parameters of adherent cell surfaces by magnetic bead microrheometry. *Biophysical Journal*, 75(4):2038, 1998.

[6] B. Rubinstein, M.F. Fournier, K. Jacobson, A.B. Verkhovsky, and A. Mogilner. Actin-myosin viscoelastic flow in the keratocyte lamellipod. *Biophysical Journal*, 97(7):1853, 2009.

[7] Evan Evans and Erich Sackmann. Translational and rotational drag coefficients for a disk moving in a liquid membrane associated with a rigid substrate. *J. Fluid Mech*, 194:553–561, 1988.

[8] Y. Mori, A. Jilkine, and L. Edelstein-Keshet. Wave-pinning and cell polarity from a bistable reaction-diffusion system. *Biophysical Journal*, 94(9):3684, 2008.

[9] Marten Postma, Leonard Bosgraaf, Harriët M Loovers, and Peter JM Van Haastert. Chemotaxis: signalling modules join hands at front and tail. *EMBO Reports*, 5(1):35–40, 2004.